A one-track model for spatiotemporal coordination of *Bacillus subtilis* septal cell wall synthesis

Kevin D. Whitley[1*], James Grimshaw[1], Eleni Karinou[1], Phillip J. Stansfeld[2,3], Séamus Holden[2*]

[1]Centre for Bacterial Cell Biology, Biosciences Institute, Faculty of Medical Sciences, Newcastle University, Newcastle upon Tyne, United Kingdom
[2]School of Life Sciences, University of Warwick, Coventry, United Kingdom
[3]Department of Chemistry, University of Warwick, Coventry, United Kingdom

[*]Corresponding authors: kevin.whitley@newcastle.ac.uk, seamus.holden@warwick.ac.uk

Abstract

Bacterial cell division requires synthesis of a septal peptidoglycan (sPG) wall across the middle of the cell. This is accomplished by the divisome synthesis complex in coordination with numerous other division proteins—such as the essential tubulin homolog FtsZ—but the molecular mechanism of its spatiotemporal regulation remains unclear. Here, we investigate the dynamics of sPG synthesis in the model Gram-positive bacterium *Bacillus subtilis* using live-cell single-molecule imaging of the divisome transpeptidase PBP2B. In contrast to previous models for division, we show that there is a single population of processively-moving PBP2B molecules whose motion is driven by peptidoglycan synthesis and is not associated with FtsZ treadmilling. However, although the motions of PBP2B and FtsZ are asynchronous, we demonstrate that processive PBP2B motion is regulated by FtsZ treadmilling. Additionally, we provide evidence that the divisome synthesis complex is multimeric. Our results support a new model for division in *B. subtilis* where a multimeric synthesis complex follows a single track dependent on sPG synthesis whose activity is regulated by FtsZ treadmilling.

Introduction

Cell division is a basic requirement for bacterial life and a major antibiotic target. At a molecular level, division is a remarkable feat of engineering by the bacterial cell: a set of nanoscale proteins must cooperate over large distances to build a micron-scale cross-wall (septum) across the middle of the cell against heavy outward pressure. Many of the proteins involved are highly conserved across the bacterial domain, including the septal peptidoglycan (sPG) synthases that insert new cell wall material into the ingrowing septum and the cytoskeletal tubulin homolog FtsZ[1]. FtsZ forms short filaments that move around the division septum by treadmilling[2–5] – a type of motion where monomers bind one end of a filament at the same rate they unbind the opposite end, causing the filament to move forward even though monomers remain stationary. In contrast, sPG synthases are part of a larger divisome synthesis complex[6] that does not treadmill, but instead moves processively around the division ring[2,3,5,7].

Several models have been proposed to explain how these proteins cooperate to enact division despite such different motion patterns[8]. We previously proposed a model where FtsZ treadmilling drives septal constriction in *B. subtilis* as a coupled cytoskeleton-synthase complex[2]. However, subsequent work in both *Staphylococcus aureus* and *B. subtilis* showed that FtsZ treadmilling is dispensable after constriction has initiated[4,9], and a study in *Streptococcus pneumoniae* showed that the motions of divisome synthesis complexes and FtsZ filaments are uncoupled[5]. Subsequent work has supported a model for division in *Escherichia coli* and *Caulobacter crescentus* where the synthase complex moves on two 'tracks': an FtsZ-track where inactive synthase complexes are distributed around the division septum and an sPG-track where synthase complexes build the cell wall independently of FtsZ[10–13]. According to this model, an activating protein (FtsN in *E. coli* and FzlA in *C.*

crescentus) is required to initiate active sPG synthesis on the sPG-track[13,14]. However, it is unclear how far this model generalises across the bacterial domain, as many species lack a known activator of cell division.

Here, we investigated the dynamics of the divisome synthesis complex and its coordination with FtsZ in *B. subtilis.* We imaged the divisome transpeptidase PBP2B at a single-molecule level around the entire division septum by orienting cells vertically in bacteria-shaped holes[9,15]. In contrast to predictions of the coupled-complex and two-track models, we found a single population of processively-moving PBP2B that is dependent on sPG synthesis and not associated with FtsZ treadmilling. However, although the motions of PBP2B and FtsZ are asynchronous, we found that the speeds of processive PBP2B molecules are partially dependent on FtsZ treadmilling. Additionally, we provide evidence that the divisome synthesis complex is multimeric. Our results support a new model for division in *B. subtilis* where a multimeric divisome synthesis complex follows a single track dependent on sPG synthesis whose activity is regulated by FtsZ treadmilling.

Results

Processive motion of the divisome synthesis complex depends on sPG synthesis.

We created a model of the *B. subtilis* divisome core complex (consisting of the proteins PBP2B, FtsW, FtsL, DivIB, and DivIC) using AlphaFold2 Multimer (Methods; Supplementary Figure 1), showing close agreement with the recent cryo-EM structure of homologous proteins from *Pseudomonas aeruginosa*[6]. Since a recent study showed that these five proteins move together as a complex *in vivo*[7], we decided to follow the overall motion dynamics of the divisome synthesis complex by tracking the well-characterised transpeptidase PBP2B. We constructed a strain that expresses a previously-characterized HaloTag fusion of PBP2B as a functional sole copy[2] (Methods; Supplementary Table 1) with an induction level that yielded near-native cell morphology (Supplementary Figure 2). To identify division septa, in addition to unlabelled native FtsZ our strain expresses GFP-FtsZ from an ectopic locus at low levels that do not interfere with cellular growth (Methods; Supplementary Figure 3).

To image single-molecule dynamics of PBP2B around the septum throughout division, we used smVerCINI (single-molecule Vertical Cell Imaging by Nanostructured Immobilisation), a method we developed for single-molecule imaging in rod-shaped cells by confining cells vertically in nanofabricated micro-holes[16] (Figure 1a). For single-molecule resolution, we sparsely labelled cells with JFX554 HaloTag ligand[17] (Methods) and loaded them into agarose micro-holes as described previously[9,15]. We identified division rings using the dilute GFP-FtsZ signal, and then imaged single-molecule dynamics of HaloTag-PBP2B (HT-PBP2B) in rich media at 30°C (Methods; Figure 1b, c; Supplementary Videos 1 and 2). The resulting distribution of speeds shows three populations: an immobile population (~0 nm/s), a processive population (~13 nm/s) (Figure 1f), and a broad fast moving population (>100 nm/s) that becomes visible when speeds are plotted on a logarithmic scale (Figure 1f inset).

We considered that the immobile population could represent molecules bound to the middle of treadmilling FtsZ filaments, as suggested previously for FtsW in *E. coli*[11]. However, the mean lifetime of the HT-PBP2B immobile tracks (48 ± 3 s; Supplementary Figure 4) is substantially longer than the reported lifetime of FtsZ monomers at the division septum in *B. subtilis* (8.1 s)[7], making this situation unlikely. Due to the long lifetime of this population, we speculate that the immobile population may be bound to the cell wall.

We wondered if the synthesis complex requires sPG synthesis for processive motion. To test this, we imaged the motion of HT-PBP2B immediately after treating cells with an excess (20 µg/mL) of penicillin G, which directly binds the enzyme's catalytic site and prevents transpeptidation. This abolished the processive population (13.4 nm/s; 95% CI [12.7, 14.1]), leaving only immobile and diffusive tracks (Figure 1d, g; Supplementary Videos 3 and 4). We repeated the experiment with fosfomycin, a separate class of antibiotic that inhibits the synthesis of lipid II, the substrate for cell

wall synthesis[18]. As with penicillin G, immediately after treatment with an excess (500 µg/mL) of fosfomycin, the processive population of HT-PBP2B vanished (Figure 1e, h; Supplementary Videos 5 and 6). We conclude that processive motion of the synthesis complex requires sPG synthesis.

We next wondered what the broad fast-speed population was. This population resulted from short back-and-forth tracks that appeared to show diffusive rather than processive motion (Supplementary Figure 5a). These tracks were often located at larger radii than immobile or processive tracks (Supplementary Figure 5b), suggesting that they are not typically present at the septal leading edge and therefore unlikely to be involved in sPG synthesis. We were initially surprised to find an apparently diffusive population during our experiments, as we expected diffusive motion to be fast enough to be blurred out during our long (1 s) acquisition interval. Since linear speeds did not represent this population well, we instead measured the mean-squared displacements (MSDs) of these tracks and fitted an anomalous diffusion model to them (Methods; Supplementary Figure 5c-f). The mean effective diffusion coefficient (D_{eff} = 6.5×10^{-3} ± 0.5×10^{-3} µm^2/s) and diffusion exponent (α = 0.78 ± 0.03) we obtained indicate that these tracks represent very slow sub-diffusive behaviour. The low diffusion coefficient is similar to that previously measured for the *E. coli* elongasome transpeptidase PBP2[19], and suggests that the HT-PBP2B molecules in this motion state are part of large complexes that diffuse along the cell membrane

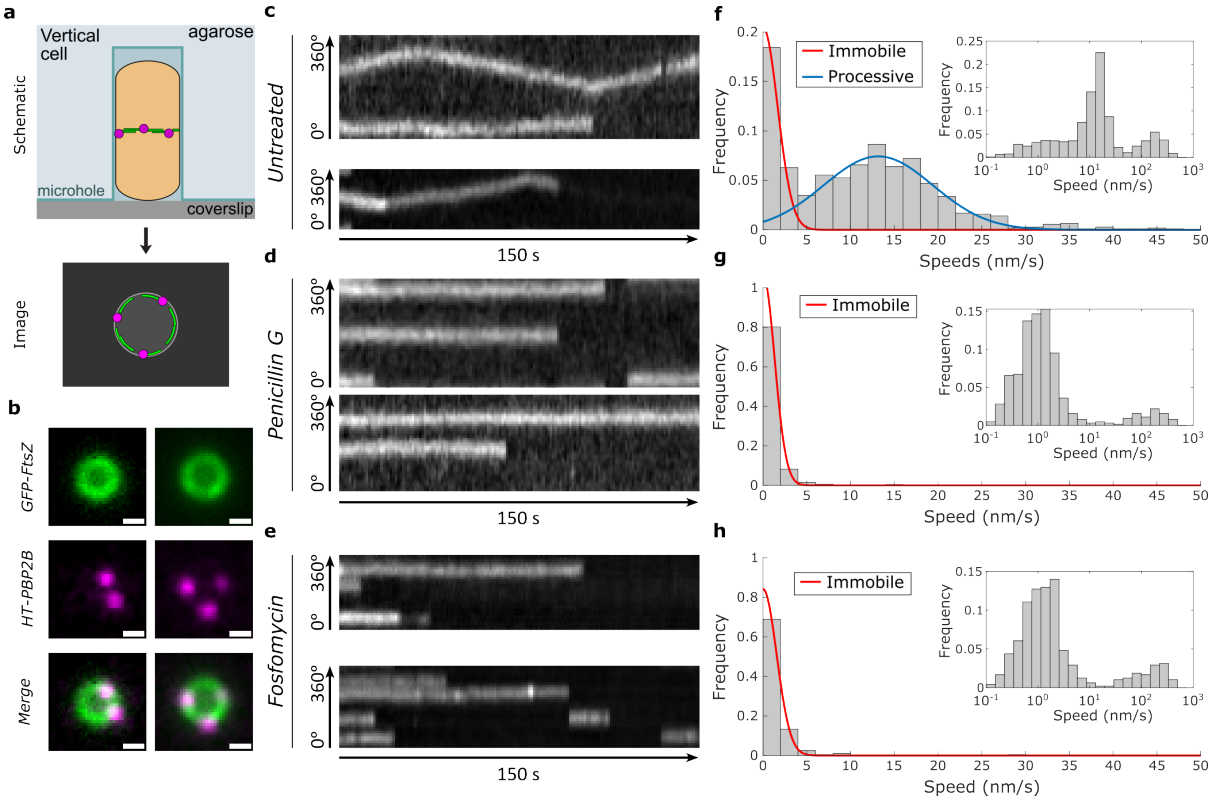

Figure 1. Two-colour smVerCINI imaging shows a single processive population of HT-PBP2B that is associated with sPG synthesis. (a) Schematic of two-colour smVerCINI experimental setup. A *B. subtilis* cell (orange) is oriented vertically in a microhole made of agarose (light blue), adjacent to a microscope coverslip (grey). By orienting the cell vertically, the division proteins FtsZ (green) and PBP2B (magenta) can be imaged in a single microscope imaging plane. **(b)** Example images of two vertically trapped cells. GFP-FtsZ (green) is expressed at a low level for use as a septal marker, while HT-PBP2B is labelled sub-stoichiometrically with JFX554 HaloTag ligand[17] so that single molecules can be easily observed. Scale bars: 500 nm. **(c)** Example radial kymographs of HT-PBP2B motion from smVerCINI videos in untreated cells. Diagonal lines result from processive motion, while horizontal lines result from lack of motion. **(d, e)** Example radial kymographs of HT-PBP2B motion from smVerCINI videos in cells treated with 20 µg/mL penicillin G or 500 µg/mL fosfomycin. **(f)** Histogram of HT-PBP2B speeds in untreated cells. Red and blue lines show fits to the data (Methods). *Inset*: Histogram of speeds plotted on logarithmic x axis, showing three populations. **(g, h)** Histograms of speeds in cells treated with penicillin G or fosfomycin. Red lines show fits to the data (Methods). *Insets*: Histograms of speeds plotted on logarithmic x axis, showing two populations. All examples in **c-h** are from cells grown in rich media at 30°C.

The divisome synthesis complex and FtsZ move asynchronously.

Our results are not consistent with either the coupled-complex[2] or two-track[11] models. Both models predict that there exists at least one processive population of synthesis complexes that move at the same speed as treadmilling FtsZ filaments[2,11], but the speed of the processive HT-PBP2B population (13.4 nm/s; 95% CI [12.7, 14.1]) (Figure 1f) does not match what we previously measured for FtsZ treadmilling (40.0 nm/s; 95% CI [26.0, 53.9])[9] under identical growth conditions (rich media, 30°C). Furthermore, in contrast to predictions from the two-track model[11], we do not observe the emergence of an FtsZ-associated speed population of HT-PBP2B after treating cells with penicillin G or fosfomycin (Figure 1g, h).

Next, we investigated whether the asynchronous motions of synthesis complexes and FtsZ treadmilling are a general feature in *B. subtilis* by repeating our measurements under different growth conditions (Figure 2a). Our results show that HT-PBP2B speeds depended on both media composition and temperature: processive molecules moved faster in rich media or 37°C than in minimal media or 30°C (blue lines in Figure 2a). Under most growth conditions tested, the speeds of processive HT-PBP2B molecules do not match the speeds of FtsZ treadmilling measured under identical conditions[9] (green dotted lines in Figure 2a). However, under the fastest growth condition (rich media, 37°C) HT-PBP2B processive speeds overlap substantially with FtsZ treadmilling speeds. Notably, this was the growth condition under which single-molecule tracking of HT-PBP2B was performed previously[2]. The similarity of speeds between FtsZ treadmilling and HT-PBP2B processive motion in those conditions led us to initially propose that the two systems moved together as a coupled complex. Our results instead indicate that this overlap in speeds is a coincidence arising only under the fastest growth condition (Figure 2a).

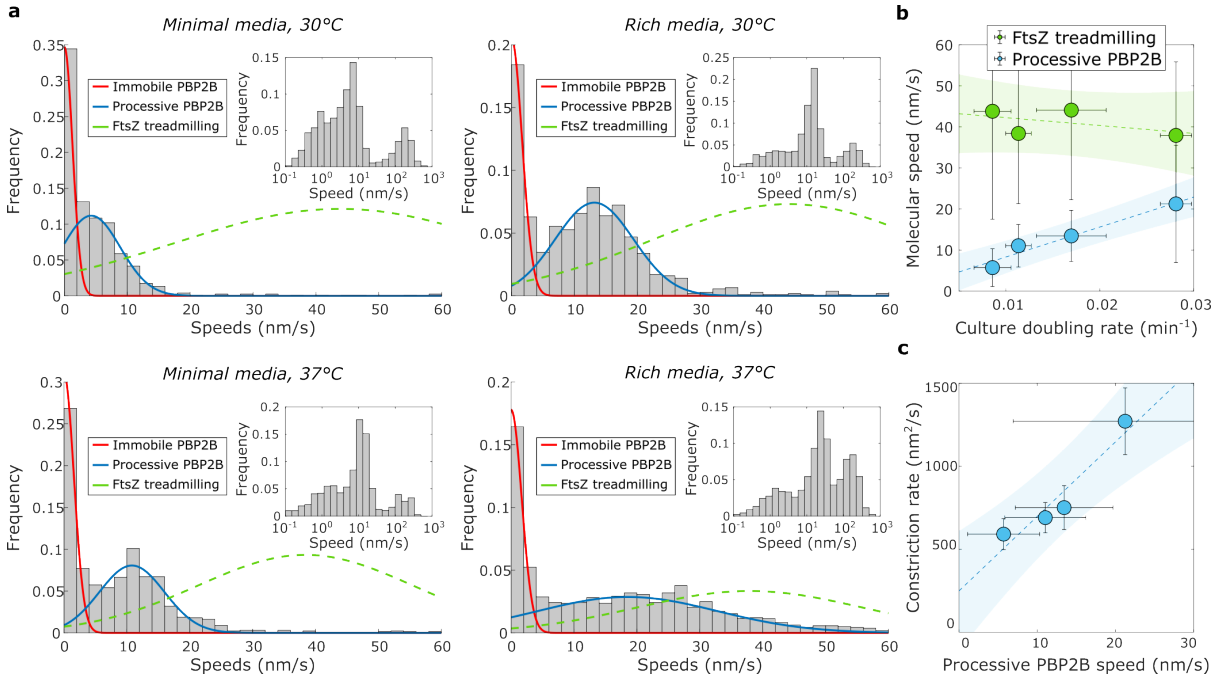

Figure 2. PBP2B and FtsZ move asynchronously. (a) Histograms of HT-PBP2B speeds across growth conditions. Red and blue lines show fits to the data (Methods). Green dotted lines show Gaussian distributions based on the mean and variance of FtsZ treadmilling speeds measured under the same growth conditions, scaled to match the height of the processive HT-PBP2B population (data from Whitley et al. 2021[9]). *Insets*: Histograms of speeds plotted on logarithmic x axes, showing three populations. **(b)** Correlation between culture doubling rates and speeds of FtsZ treadmilling and processive HT-PBP2B. Dotted lines show linear fits to the data. Shaded regions show 95% confidence bands. Error bars are SD. **(c)** Correlation between processive HT-PBP2B speeds and septal constriction rate. Septal constriction rates under these conditions are from Whitley et al. 2021[9]. Dotted line shows a linear fit to the data. Shaded region shows 95% confidence bands. Error bars are SD.

We found that processive HT-PBP2B speeds are correlated with cell growth rate (doubling rate in liquid culture), while FtsZ treadmilling is independent of growth rate (Figure 2b). We speculate that

faster growth conditions results in more rapid production of cell wall substrate (lipid II), leading to a higher rate of sPG incorporation reactions and hence higher synthesis complex speeds. We further found that processive HT-PBP2B speeds are correlated with the rate of septal constriction, which we measured previously under identical conditions[9] (Figure 2c). It is possible that higher synthesis complex speeds lead to more sPG added to the ingrowing septum per unit time, thereby resulting in a higher rate of septal constriction.

Processive motion of the divisome synthesis complex partially depends on FtsZ treadmilling.

Our finding that FtsZ and HT-PBP2B move asynchronously suggests that synthesis complexes are independent of FtsZ treadmilling in *B. subtilis*. To test this directly, we measured the dynamics of HT-PBP2B in the absence of FtsZ treadmilling. We treated cells with 10 µM PC190723, an antibiotic that specifically binds to FtsZ[20] and arrests treadmilling[2] across all stages of division within seconds of treatment[9]. HT-PBP2B still showed processive motion (Figure 3a, c; Supplementary Videos 7 and 8), but the speeds were slower than in untreated cells (8.1 nm/s; 95% CI [7.0, 9.4] treated vs. 13.4 nm/s; 95% CI [12.7, 14.0] untreated). This is a stark difference from the penicillin G- or fosfomycin-treated cells, where the processive population was abolished (Figure 1g, h).

We wondered if this drop in speeds was specific to treatment with PC190723, which is a strong perturbation due to its sudden and total arrest of FtsZ treadmilling. We therefore tried a similar genetic perturbation by using an FtsZ mutant (FtsZ^{G106S}) that is competent for division but has reduced treadmilling speed[2] and produces a long-cell phenotype (Methods; Supplementary Table 1; Supplementary Figure 6). The speed distribution for HT-PBP2B in this mutant strain was similar to that observed with PC190723-treated wild-type cells (Figure 3b, d; Supplementary Videos 9 and 10). This suggests that any substantial disruption to FtsZ treadmilling has similar effects on synthesis complex motion (Figure 3e), in contrast to the linear relation between their speeds proposed previously[2].

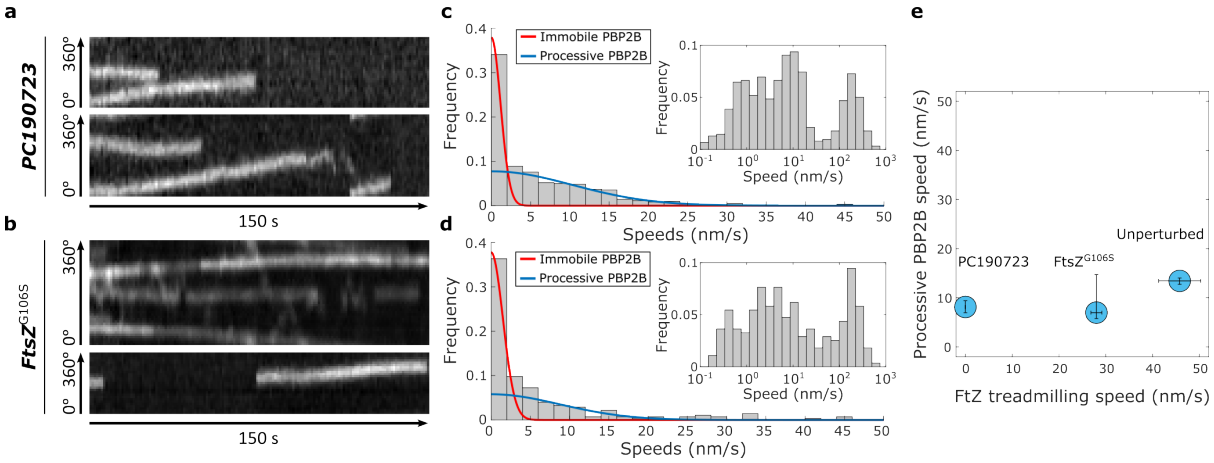

Figure 3. PBP2B motion partially depends on FtsZ treadmilling. (a) Example radial kymographs of HT-PBP2B motion from smVerCINI videos in cells treated with 10 µM PC190723. **(b)** Example radial kymographs in cells expressing the treadmilling-impaired mutant FtsZ^{G106S}. **(c)** Histogram of speeds in cells treated with PC190723. **(d)** Histogram of speeds in FtsZ^{G106S} cells. Red and blue lines to both histograms show fits to the data (Methods). *Insets*: Histograms of speeds plotted on logarithmic x axes, showing three populations. **(e)** Relation between FtsZ treadmilling speeds and processive HT-PBP2B speeds. Data for FtsZ^{G106S} treadmilling speed from Bisson-Filho et al. 2017[2]. Error bars are 95% CI.

The divisome synthesis complex is multimeric.

During this study, we observed many cases where the fluorescence intensities of HT-PBP2B spots showed discrete drops to half their value (Figure 4a, b; Supplementary Videos 2 and 11), indicating the presence of two copies of the fluorescently-labelled protein. We also observed multiple occasions where such intensity drops occurred during motion and even after direction changes (Figure 4a, b; Supplementary Figure 7), strongly suggesting that multiple monomers of HT-PBP2B are moving together as part of a larger complex. Due to the sub-stoichiometric nature of the labelling method, we

cannot precisely quantify the number of HT-PBP2B molecules in a given complex, although we have observed rare cases with even three or four such drops in intensity (Supplementary Figure 8).

Surprisingly, we also observe cases where the fluorescence intensity signal shows discrete jumps to twice their value (Figure 4c, d; Supplementary Figure 9; Supplementary Videos 12 and 13). We observe these discrete jumps in both immobile and processive tracks. This suggests that the oligomeric state of synthesis complexes is dynamic, where new PBP2B molecules can bind to both active and inactive complexes. It is currently unclear what effect stoichiometry has on divisome activity and dynamics. This will be followed up in future work.

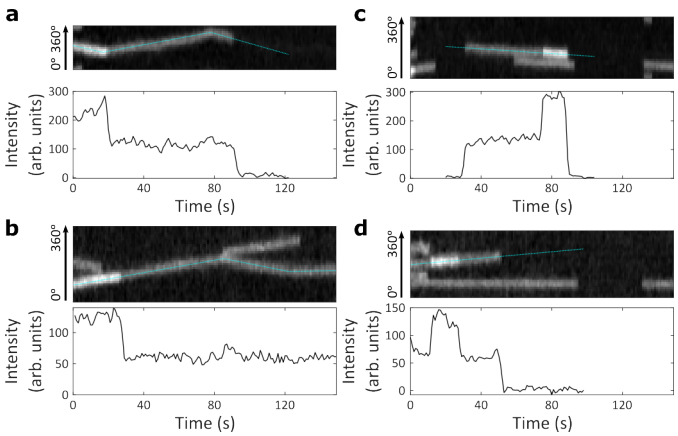

Figure 4. PBP2B is part of dynamic multimeric complexes. (a, b) *Top:* Example kymographs of HT-PBP2B motion from smVerCINI videos showing discrete drops in fluorescence intensity mid-track. *Bottom:* Intensity traces for the tracks designated by dotted cyan lines overlaid on kymographs. Both traces are from cells grown in rich media at 30°C. **(c, d)** *Top:* Example kymographs showing discrete jumps in fluorescence intensity mid-track. *Bottom:* Intensity traces for the tracks designated by dotted cyan lines overlaid on kymographs. Both traces are from cells grown in minimal media at 30°C.

Discussion

Our results show that a multimeric divisome synthesis complex in *B. subtilis* follows a single track dependent on sPG synthesis and regulated by—but asynchronous with—FtsZ treadmilling. This sharply contrasts with two prominent models for bacterial cell division[2,11], which predict the existence of a processive population of synthesis complexes associated with FtsZ treadmilling.

We propose a new model for division in *B. subtilis* where FtsZ filaments define the track for sPG synthesis, and active synthesis complexes move independently along this track (Figure 5). Treadmilling by FtsZ is a requirement for an ordered, linear division ring. More specifically, in order to form and maintain a smooth ring, FtsZ filaments need to be both 'mortal' and motile– that is, they need to be able to dynamically reorganise by depolymerization-driven treadmilling[21]. In this model the track becomes disordered when FtsZ treadmilling is perturbed, leading to non-linear synthesis complex motion and slower observed speeds. There are several possible ways the synthesis complexes could use FtsZ filaments as a track. Similar to what has been proposed in *E. coli*, they could be guided by weak interactions with FtsAZ[12]. Alternatively, as FtsZ is known to generate a constrictive force on membranes[22,23] filaments may create a local membrane deformation that lowers the energy barrier for synthesis complexes to move forward[24].

Our finding that the motions of synthesis complexes and FtsZ are asynchronous is consistent with previous measurements in *S. pneumoniae*[5] and work performed in parallel to this study in *S. aureus*[25]. Our discovery that synthesis complexes retain processive motion in the absence of FtsZ treadmilling also agrees with previous findings in both *S. aureus* and *B. subtilis* that septal constriction continues in the absence of FtsZ treadmilling if it has already initiated[4,9]. This suggests that these species—all members of the phylum Bacillota (Firmicutes)—share a similar mechanism for division. It is possible that the two-track model proposed for *E. coli* and *C. crescentus*—both members of the phylum Pseudomonadota (Proteobacteria)—represents a special case arising from requirements unique to this bacterial clade, such as a thinner PG layer or sparser network of FtsZ filaments.

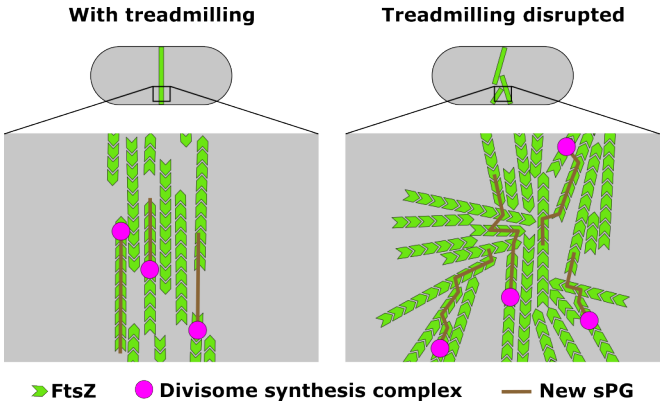

Figure 5. Model for sPG synthesis regulation by FtsZ treadmilling. *Left*: Treadmilling by FtsZ filaments (monomers shown as green chevrons) produces a linear track around the circumference of the cell (grey). Divisome synthesis complexes (magenta) use this as a track to synthesize sPG (brown). *Right*: When FtsZ treadmilling is disrupted, divisome synthesis complexes continue synthesizing sPG, but move along a disordered, fragmented track.

Previously, our collaborators observed that arrest of FtsZ treadmilling by the antibiotic PC190723 abolished processive HT-PBP2B motion[2], but here we find that the effect of arresting FtsZ treadmilling is to slow HT-PBP2B processive motion rather than stop it. It is possible that the difference in these results comes from the different imaging geometries used. Previously, HT-PBP2B was imaged using Total Internal Reflection Fluorescence (TIRF) illumination, which only captures a thin slice of the division ring near the microscope coverslip, preventing observation of the later stages of constriction. This may have biased observations toward HT-PBP2B molecules in the population of Z-rings that had not initiated constriction prior to PC190723 treatment, and therefore were not capable of division. In that case, synthesis complexes may have remained inactive and therefore immobile.

We have shown that perturbations to FtsZ treadmilling leads to slower speeds for processive synthesis complexes. The reduction in speeds upon total arrest of FtsZ treadmilling (~40%) correlates with the reduction in septal constriction rate (by 14-33%, depending on growth conditions) we previously observed under similar conditions[9]. This is corroborated by our finding that synthesis complex speeds are correlated with septal constriction rate (Figure 2c). However, work performed in parallel to this study in *S. aureus* found that synthesis complex speeds and septal constriction rate are not affected by FtsZ treadmilling[25]. In contrast to both of these studies, previous work in *S. pneumoniae* found a minor (~25%) reduction in synthesis complex speeds when FtsZ treadmilling was severely perturbed, and no effect from a smaller perturbation[5]. This suggests that although these three species may share a similar mechanism for division, there may remain minor differences, which could arise from changes in the interaction strength of FtsZ subunits with the rest of the divisome.

We also found evidence that the divisome synthesis complex is multimeric, in support of the 'stoichiometric divisome' hypothesis[26]. The recently published structure of the highly conserved divisome core complex in *Pseudomonas aeruginosa* consists of FtsI (PBP2B homologue) in a complex with FtsW, FtsB (DivIC homologue), FtsL and FtsQ (DivIB homologue)[6]. As the stoichiometry of PBP2B homologue FtsI with each of the other components is 1:1, this suggests that each synthesis complex contains multiple copies of each protein. The multimeric nature of this complex may also explain the abrupt changes in direction we observe in single-molecule tracks (Figure 1c). Such bidirectional motion can result from multiple motor proteins in a complex pulling in opposite directions, as is well-known for motor proteins moving along the eukaryotic cytoskeleton[27] and more recently the elongasome of *B. subtilis*[16]. Inclusion in a large multimeric complex may also explain the very low effective diffusion coefficient we measured for HT-PBP2B (Supplementary Figure 4e).

Acknowledgements
We would like to acknowledge Ethan Garner (Harvard) and Ling Juan Wu (Newcastle) for sharing strains, Luke Lavis (Janelia Farm) for providing us with JFX554 HaloTag ligand and Stuart Middlemiss (Newcastle) for advice with cloning. We would also like to thank Mariana Pinho (ITQB NOVA) and Jie Xiao (Johns Hopkins) for helpful discussions. S.H., K.D.W., J.G., and E.K. acknowledge funding support by a Newcastle University Research Fellowship, a Wellcome Society Sir Henry Dale Fellowship grant number [206670/Z/17/Z], and a BBSRC 19ALERT mid-range equipment initiative grant [BB/T017570/1]. Research in P.J.S.'s lab was funded by Wellcome (208361/Z/17/Z), the MRC (MR/S009213/1) and BBSRC (BB/P01948X/1, BB/R002517/1 and BB/S003339/1).

Author contributions
K.D.W. and S.H. designed the research; K.D.W. performed the experiments; K.D.W., J.G., and E.K. constructed and characterised bacterial strains; K.D.W. analysed the data. P.J.S. performed protein structure predictions; K.D.W. and S.H. wrote the manuscript with input from all authors.

Competing interests
The authors declare no conflict of interest.

Methods

Divisome complex modelling. The divisome complex was modelled by AlphaFold2, using ColabFold (v1.3.0) and AlphaFold-Multimer (v2). The sequences were downloaded from the UniProtKB database and included five divisome protein sequences (Q07868 (PBP2B); Q07867 (FtsL); O07639 (FtsW); P16655 (DivIB); P37471 (DivIC)).

Bacterial strains and growth conditions. Strains used in this study are listed in Supplementary Table 1. Strains were streaked from -80°C glycerol stocks onto nutrient agar (NA) plates containing the relevant antibiotics and 1 mM IPTG and grown overnight at 37°C. Single colonies were transferred to liquid starter cultures in either PHMM medium[2] or Time-Lapse Medium[28] (TLM) with 100 µM IPTG, shaking at 200 rpm overnight at either 22°C (PHMM) or 30°C (TLM). The next day, PHMM starter cultures were diluted to OD_{600} = 0.05 in fresh PHMM, while TLM starter cultures were diluted OD_{600} = 0.1 in Chemically-Defined Medium (CDM)[28]. These liquid cultures were grown at 30 or 37°C with 100 µM IPTG and 0.075% xylose until they reached $0.3 < OD_{600} < 0.6$. When necessary, antibiotics were used at the following concentrations: spectinomycin 60 µg/mL, erythromycin 1 µg/mL, lincomycin 25 µg/mL, 6 µg/mL tetracycline.

Strain construction. All strains used with smVerCINI experiments harboured a deletion of the *hag* gene, as this has been shown to reduce the chaining phenotype in *B. subtilis* cells and thereby increase loading into micro-holes[9,15].

SH142 (PY79 Δ*hag, amyE*::*spc*-P_{xyl}-*gfp-ftsZ*) was constructed by transforming SH211 with genomic DNA extracted from strain 2020 using standard protocols[29].

SH147 (PY79 Δ*hag, pbpB*::*erm*-$P_{hyperspank}$-*HaloTag-15aa-pbpB*, *amyE*::*spc*-P_{xyl}-*gfp-ftsZ*) was constructed by transforming SH142 with a PCR product obtained from bGS31 genomic DNA. The primer pair ftsL Fw/ spoVD Rev (Supplementary Table 2) were used to amplify the region around the *pbpB* gene using bGS31 genomic DNA as a template. The primer pair ftsL Fwd/ pbp2B Rev (Supplementary Table 2) was used to confirm insertion of the *HaloTag* gene in the transformant. Insertion was also confirmed by Sanger sequencing.

SH203 (PY79 Δ*hag*, *pbpB*::*erm*-$P_{hyperspank}$-*HaloTag-15aa-pbpB*, *ftsZ*Ω*ftsZ(G106S) (tet)*, *amyE*::*spc*-P_{xyl}-*gfp-ftsZ*) was constructed by transforming SH147 with genomic DNA extracted from strain Z-G106S (gifted by Ethan Garner). The point mutation G106S was confirmed by Sanger sequencing.

Bacterial strain characterisation. Strains were characterised by growth in liquid culture (Supplementary Figures 3 and 6) and cell morphology analysis (Supplementary Figures 2 and 6).

Growth curves. *B. subtilis* PY79 and variant strains were grown in liquid starter cultures overnight in LB at 30°C with required inducers (100 µM IPTG for SH147 and SH203). To measure culture growth across [IPTG] (Supplementary Figure 3), SH147 overnight cultures were washed twice in LB to remove inducer. Cultures were then diluted to OD_{600} = 0.05 in LB with variable inducer concentrations, and 200 µL of each dilution was added to a 96-well microtiter plate. Growth was monitored for 15 h using a FLUOStar OPTIMA plate reader (BMG Labtech). Growth curves for each condition were performed in triplicate.

Cell morphology analysis. *B. subtilis* PY79 and variant strains were grown in liquid starter cultures overnight in PHMM at 22°C or 30°C with required inducers (100 µM IPTG for SH147 and SH203). To measure cell morphology across [IPTG] (Supplementary Figure 2), SH147 overnight cultures were washed twice in PHMM to remove inducer. Cultures were then diluted to OD_{600} = 0.05 in PHMM with variable [IPTG]. Once the cultures had reached $0.3 < OD_{600} < 0.6$, Nile Red was added to cells and incubated at growth temperatures for 5 min. 0.5 µL of cell culture was then spotted on 1.2-2% agarose pads of PHMM with variable [IPTG], prepared as described previously[28]. Cells were imaged using a 561 nm laser or 550 nm LED, and cell lengths were manually determined using ImageJ.

smVerCINI. smVerCINI was set up as described previously for VerCINI[9,15]. Briefly, agarose microholes were formed by pouring molten 6% agarose onto a nanofabricated silicon array consisting of micropillars with widths 1.0-1.3 µm and heights 6.8 µm. Patterned agarose was transferred into a Geneframe (Thermo Scientific) mounted on a glass slide, and excess agarose was cut away to ensure sufficient oxygen. Labelled cells at $0.3 < OD_{600} < 0.6$ were concentrated 100× by centrifugation and added onto the agarose pad. Cells were then loaded into the microholes by centrifuging the mounted agarose pad with concentrated cell culture in an Eppendorf 5810 centrifuge with MTP/Flex buckets. Unloaded cells were rinsed off with excess media. In experiments where cells were treated with antibiotic (Figures 1d, 1e, and 3a), 5 µL of media laced with antibiotic was added to the top of loaded cells and allowed to absorb for ~1 min prior to sealing with a coverslip and imaging.

Imaging was done by first recording a single frame of GFP-FtsZ using the 488 nm laser to identify division rings. Immediately following this, a time-lapse of HT-PBP2B dynamics was recorded using the 561 nm laser. Following fluorescence imaging, a short bright-field video was recorded to identify any cells that were improperly trapped in micro-holes. Microscopy acquisition parameters are listed in Supplementary Table 3.

HaloTag labelling with JFX554 dye. Single-molecule labelling of HT-PBP2B was done by incubating strain SH147 or SH203 with either 100 pM (minimal media) or 250 pM (rich media) JFX554 HaloTag ligand for 15 min. Cells were washed once with fresh media before imaging. JFX554 HaloTag ligand was a gift from Luke Lavis (Janelia Farm)[17].

Microscopy. Power densities, exposure times, and other key parameters are listed for each microscopy experiment in Supplementary Table 3. All imaging was done using either a Nikon Eclipse Ti2 inverted fluorescence microscope or a bespoke inverted microscope.

Nikon Eclipse Ti2. Cells were illuminated with 488 nm and 561 nm laser illumination. A 100× TIRF objective (Nikon CFI Apochromat TIRF 100XC Oil) was used for imaging and a Kinetix sCMOS camera

(Teledyne Photometrics) was used with effective pixel size of 65 nm/pixel. Cells were illuminated using HiLO to minimise background using an objective TIRF module.

Bespoke microscope. Cells were illuminated with a 488 nm laser (Obis) and a 561 nm laser (Obis). A 100× TIRF objective (Nikon CFI Apochromat TIRF 100XC Oil) was used for all experiments. A 200 mm tube lens (Thorlabs TTL200) and Prime BSI sCMOS camera (Teledyne Photometrics) were used for imaging, giving an effective pixel size of 65 nm/pixel. Imaging was done with a custom-built ring-TIRF module operated in ring-HiLO using a pair of galvanometer mirrors (Thorlabs) spinning at 200 Hz to provide uniform, high SNR illumination[30].

Image processing and analysis. Videos were denoised using the GPU-accelerated ImageJ plugin PureDenoise-GPU[16].

Cells with mature or constricting division rings in focus were chosen using the first GFP-FtsZ image acquired in the imaging sequence described above. The short bright-field videos of each field of view acquired after fluorescence imaging were then used to filter out any of these cells that were improperly trapped in the holes.

Previously developed software[9,15] was used to subtract the cytoplasmic background signal and produce radial kymographs. Due to chromatic aberration, the HT-PBP2B signal itself was used for fitting and extracting radial kymographs rather than the single GFP-FtsZ frame. Due to the difficulty of fitting a circle to these sparsely-labelled rings, the maximum intensity projections of the HT-PBP2B videos were used for fitting, and each fit was manually inspected to confirm it was adequate.

Measurements of filament speed and processivity were performed manually by kymograph analysis, annotating filaments as lines in ImageJ and then measuring the angle via ImageJ script. For visual display purposes, kymographs represented here in some cases have the circle origin (0°/360°) rotated around the division ring so that single-molecule tracks are appropriately shown as continuous.

Speed distribution analysis. Speed histograms were fitted to a sum of Gaussian distributions. For most histograms, a sum of three Gaussian distributions was used, but in the cases of penicillin G and fosfomycin treatment (Figure 1g, h) these fits yielded two overlapping distributions at 0 nm/s. In these two cases, then, a sum of two Gaussian distributions was used rather than three. As one population was expected to represent fully immobile molecules with speed of 0 nm/s, this one parameter was fixed in all cases. Processive HT-PBP2B speeds were determined from these fits by calculating the first moment of the Gaussian distribution fitting the processive population. 95% confidence intervals were obtained by bootstrapping.

Single-particle tracking and MSD analysis. For analysis of the diffusive HT-PBP2B population, single molecules were detected and tracked using TrackMate[31] with linking distance of 0.5 µm, 5 frame gaps, 0.5 µm gap-closing distance. Only tracks >10 frames long were used for further analysis. Bespoke Matlab code was used to plot tracks in polar coordinates and fit mean-squared displacements (MSDs) to the anomalous diffusion model $MSD = 4D_{eff}t^{\alpha}$, where D_{eff} is the effective diffusion coefficient and α is the anomalous diffusion exponent.

Statistics and reproducibility. All sample sizes and number of experimental replicates can be found in Supplementary Table 4.

437 **References**

438 1. Megrian, D., Taib, N., Jaffe, A. L., Banfield, J. F. & Gribaldo, S. Ancient origin and constrained
439 evolution of the division and cell wall gene cluster in Bacteria. *Nat. Microbiol.* **7**, 2114–2127
440 (2022).
441 2. Bisson-Filho, A. W. *et al.* Treadmilling by FtsZ filaments drives peptidoglycan synthesis and
442 bacterial cell division. *Science* **355**, 739–743 (2017).
443 3. Yang, X. *et al.* GTPase activity–coupled treadmilling of the bacterial tubulin FtsZ organizes septal
444 cell wall synthesis. *Science* **355**, 744–747 (2017).
445 4. Monteiro, J. M. *et al.* Peptidoglycan synthesis drives an FtsZ-treadmilling-independent step of
446 cytokinesis. *Nature* **554**, 528–532 (2018).
447 5. Perez, A. J. *et al.* Movement dynamics of divisome proteins and PBP2x:FtsW in cells of
448 *Streptococcus pneumoniae*. *Proc. Natl. Acad. Sci.* **116**, 3211–3220 (2019).
449 6. Käshammer, L. *et al.* Cryo-EM structure of the bacterial divisome core complex and antibiotic
450 target FtsWIQBL. *Nat. Microbiol.* (2023) doi:10.1038/s41564-023-01368-0.
451 7. Squyres, G. R. *et al.* Single-molecule imaging reveals that Z-ring condensation is essential for cell
452 division in Bacillus subtilis. *Nat. Microbiol.* **6**, 553–562 (2021).
453 8. Barrows, J. M. & Goley, E. D. FtsZ dynamics in bacterial division: What, how, and why? *Curr.*
454 *Opin. Cell Biol.* **68**, 163–172 (2021).
455 9. Whitley, K. D. *et al.* FtsZ treadmilling is essential for Z-ring condensation and septal constriction
456 initiation in Bacillus subtilis cell division. *Nat. Commun.* **12**, 2448 (2021).
457 10. Baranova, N. *et al.* Diffusion and capture permits dynamic coupling between treadmilling FtsZ
458 filaments and cell division proteins. *Nat. Microbiol.* **5**, 407–417 (2020).
459 11. Yang, X. *et al.* A two-track model for the spatiotemporal coordination of bacterial septal cell wall
460 synthesis revealed by single-molecule imaging of FtsW. *Nat. Microbiol.* **6**, 584–593 (2021).
461 12. McCausland, J. W. *et al.* Treadmilling FtsZ polymers drive the directional movement of sPG-
462 synthesis enzymes via a Brownian ratchet mechanism. *Nat. Commun.* **12**, 609 (2021).

463 13. Mahone, C. R. *et al. Integration of cell wall synthesis activation and chromosome segregation*
464 *during cell division in* Caulobacter. http://biorxiv.org/lookup/doi/10.1101/2022.11.05.515301
465 (2022) doi:10.1101/2022.11.05.515301.
466 14. Lyu, Z. *et al.* FtsN maintains active septal cell wall synthesis by forming a processive complex
467 with the septum-specific peptidoglycan synthases in E. coli. *Nat. Commun.* **13**, 5751 (2022).
468 15. Whitley, K. D., Middlemiss, S., Jukes, C., Dekker, C. & Holden, S. High-resolution imaging of
469 bacterial spatial organization with vertical cell imaging by nanostructured immobilization
470 (VerCINI). *Nat. Protoc.* **17**, 847–869 (2022).
471 16. Middlemiss, S. *et al. Molecular motor tug-of-war regulates elongasome cell wall synthesis*
472 *dynamics in* Bacillus subtilis. http://biorxiv.org/lookup/doi/10.1101/2023.05.10.540107 (2023)
473 doi:10.1101/2023.05.10.540107.
474 17. Grimm, J. B. *et al. Deuteration improves small-molecule fluorophores*.
475 http://biorxiv.org/lookup/doi/10.1101/2020.08.17.250027 (2020)
476 doi:10.1101/2020.08.17.250027.
477 18. Silver, L. L. Fosfomycin: Mechanism and Resistance. *Cold Spring Harb. Perspect. Med.* **7**, a025262
478 (2017).
479 19. Özbaykal, G. *et al.* The transpeptidase PBP2 governs initial localization and activity of the major
480 cell-wall synthesis machinery in E. coli. *eLife* **9**, e50629 (2020).
481 20. Haydon, D. J. *et al.* An Inhibitor of FtsZ with Potent and Selective Anti-Staphylococcal Activity.
482 *Science* **321**, 1673–1675 (2008).
483 21. Vanhille-Campos, C. *et al. Self-organisation of mortal filaments: the role of FtsZ treadmilling in*
484 *bacterial division ring formation*. http://biorxiv.org/lookup/doi/10.1101/2023.05.08.539808
485 (2023) doi:10.1101/2023.05.08.539808.
486 22. Osawa, M., Anderson, D. E. & Erickson, H. P. Reconstitution of Contractile FtsZ Rings in
487 Liposomes. *Science* **320**, 792–794 (2008).

488 23. Ramirez-Diaz, D. A. *et al.* FtsZ induces membrane deformations via torsional stress upon GTP
489 hydrolysis. *Nat. Commun.* **12**, 3310 (2021).
490 24. Holden, S. Probing the mechanistic principles of bacterial cell division with super-resolution
491 microscopy. *Curr. Opin. Microbiol.* **43**, 84–91 (2018).
492 25. Schäper, S. *et al.* Processive movement of the essential division peptidoglycan synthesis complex
493 is independent of FtsZ treadmilling and drives cell constriction in Staphylococcus aureus. *bioRxiv*
494 (2023).
495 26. Egan, A. J. F. & Vollmer, W. The stoichiometric divisome: a hypothesis. *Front. Microbiol.* **6**,
496 (2015).
497 27. Welte, M. A. Bidirectional Transport along Microtubules. *Curr. Biol.* **14**, R525–R537 (2004).
498 28. De Jong, I. G., Beilharz, K., Kuipers, O. P. & Veening, J.-W. Live Cell Imaging of Bacillus subtilis and
499 Streptococcus pneumoniae using Automated Time-lapse Microscopy. *J. Vis. Exp.* 3145 (2011)
500 doi:10.3791/3145.
501 29. *Molecular biological methods for Bacillus*. (Wiley, 1990).
502 30. Ellefsen, K. L., Dynes, J. L. & Parker, I. Spinning-Spot Shadowless TIRF Microscopy. *PLOS ONE* **10**,
503 e0136055 (2015).
504 31. Tinevez, J.-Y. *et al.* TrackMate: An open and extensible platform for single-particle tracking.
505 *Methods* **115**, 80–90 (2017).
506